Pronounced Effects of Crystal Structures on Intramolecular Electron Transfer in Mixed-Valence Biferrocenium Cations: Structural, EPR, and ^{57}Fe Mössbauer Characteristics

Teng-Yuan Dong,*[,1] Pei-Har Ho, Xiao-Qian Lai, Zhi-Wei Lin, and Kuan-Jiuh Lin[2]

Department of Chemistry, National Sun Yat-Sen University, Kaohsuing, Taiwan, and the Institute of Chemistry, Academia Sinica, Nankang, Taipei, Taiwan

Received November 5, 1999

Crystallographic properties play an important role in controlling the rate of electron transfer in mixed-valence 1′,1‴-disubstituted-biferrocenium triiodide salts. The X-ray structure of neutral 1′,1‴-dinaphthylmethylbiferrocene has been determined at 298 K. The corresponding mixed-valence 1′,1‴-dinaphthylmethylbiferrocenium triiodide exhibits two crystalline morphologies at 298 K. Dark crystals, formed when a CH_2Cl_2 solution of triiodide salt was allowed to evaporate slowly, crystallize in space group $P\bar{1}$. Dark crystals, obtained when a layer of hexane was allowed to slowly diffuse into a CH_2Cl_2 solution of triiodide salt, crystallize in monoclinic space group $P2_1/n$. The observations of the structural characteristics of 1′,1‴-dinaphthylmethylbiferrocenium triiodide are also consistent with our Mössbauer studies. The cation with space group $P\bar{1}$ shows two doublets in the variable-temperature Mössbauer spectra at temperatures below 100 K. An increase of temperature causes the two doublets to move together, resulting in an average-valence doublet at 130 K. At 300 K, the spectrum of this sample shows a single doublet which is characteristic of a valence-detrapped cation in which the electron-transfer rate exceeds $\sim 10^8$ s^{-1}. On the other hand, the cation with $P2_1/n$ phase exhibits a Mössbauer spectrum characteric of a valence-trapped cation at 300 K. Obviously, the intramolecular electron-transfer rate is quite sensitive to environment perturbations caused by different crystal packing arrangements. At 77 K, the EPR spectrum of cation with $P\bar{1}$ phase is clearly a typical axial-type spectrum with $g_{\|} = 3.16$ and $g_{\perp} = 1.91$. Surprisingly, the EPR spectrum of the cation with $P2_1/n$ phase consists of two $g_{\|}$ signals (3.67 and 2.85) and two $g_{\perp}$ signals (2.01 and 1.79). We suggest that the origin arises from the interaction of spin−spin exchange resulting from a dipole−dipole interaction that develops between cations. The syntheses, characterizations, and physical properties of mixed-valence 1′,1‴-di(4-biphenylmethyl)biferrocenium and 1′,1‴-di(9-anthracenylmethyl)biferrocenium triiodide salts are also described.

Introduction

The study of intramolecular electron transfer in mixed-valence complexes has given insight into the factors that affect rates of electron transfer in solution redox processes, solid-state materials, and biological electron-transport chains.[3−6] One of the most thoroughly studied mixed-valence compounds is biferrocenium triiodide salts.[7−25] Studies of electron transfer in the series of mixed-valence biferrocenium compounds **1** (Chart 1) revealed that the environment surrounding a cation is perhaps the most important factor in determining the rate of intramolecular electron transfer.[8−12] Compounds **1** give unusual temperature-dependent Mössbauer spec-

(1) Department of Chemistry, National Sun Yat-Sen University.
(2) Institute of Chemistry, Academia Sinica.
(3) Day, P. *Int. Rev. Phys. Chem.* **1981**, *1*, 149.
(4) Brown, D. *Mixed-Valence Compounds, Theory and Applications in Chemistry, Physics, Geology and Biology*; Reidel: Boston, MA, 1980.
(5) Creutz, C. *Prog. Inorg. Chem.* **1983**, *30*, 1.
(6) Richardson, D. E.; Taube, H. *Coord. Chem. Rev.* **1984**, *60*, 107.
(7) Hendrickson, D. N.; Oh, S. M.; Dong, T.-Y.; Kambara, T.; Cohn, M. J.; Moore, M. F. *Comments Inorg. Chem.* **1985**, *4*, 329.
(8) Dong, T.-Y.; Hendrickson, D. N.; Iwai, K.; Cohn, M. J.; Geib, S. J.; Rheingold, A. L.; Sano, H.; Motoyama, I.; Nakashima, S. *J. Am. Chem. Soc.* **1985**, *107*, 7996.
(9) Dong, T.-Y.; Hendrickson, D. N.; Pierpont, C. G.; Moore, M. F. *J. Am. Chem. Soc.* **1986**, *108*, 963.
(10) Iijima, S.; Saida, R.; Motoyama, I.; Sano, H. *Bull. Chem. Soc. Jpn.* **1981**, *54*, 1375.
(11) Nakashima, S.; Katada, M.; Motoyama, I.; Sano, H. *Bull. Chem. Soc. Jpn.* **1987**, *60*, 2253.
(12) Kai, M.; Katada, M.; Sano, H. *Chem. Lett.* **1988**, 1523.
(13) Dong, T.-Y.; Schei, C. C.; Hsu, T. L.; Lee, S. L.; Li, S. J. *Inorg. Chem.* **1991**, *30*, 2457.
(14) Dong, T.-Y.; Chou, C. Y. *J. Chem. Soc., Chem. Commun.* **1990**, 1332.
(15) Dong, T.-Y.; Schei, C. C.; Hwang, M. Y.; Lee, T. Y.; Yeh, S. K.; Wen, Y. S. *Organometallics* **1992**, *11*, 573.
(16) Webb, R. J.; Geib, S. J.; Staley, D. L.; Rheingold, A. L.; Hendrickson, D. N. *J. Am. Chem. Soc.* **1990**, *112*, 5031.
(17) Webb, R. J.; Rheingold, A. L.; Geib, S. J.; Staley, D. L.; Hendrickson, D. N. *Angew. Chem., Int. Ed. Engl.* **1989**, *28*, 1388.
(18) Dong, T.-Y.; Kambara, T.; Hendrickson, D. N. *J. Am. Chem. Soc.* **1986**, *108*, 5857.
(19) Dong, T.-Y.; Kambara, T.; Hendrickson, D. N. *J. Am. Chem. Soc.* **1986**, *108*, 4423.
(20) Jang, H. G.; Geib, S. J.; Kaneko, Y.; Nakano, M.; Sorai, M.; Rheingold, A. L.; Montez, B.; Hendrickson, D. N. *J. Am. Chem. Soc.* **1989**, *111*, 173.

10.1021/om9908884 CCC: $19.00
Publication on Web 02/24/2000

Chart 1

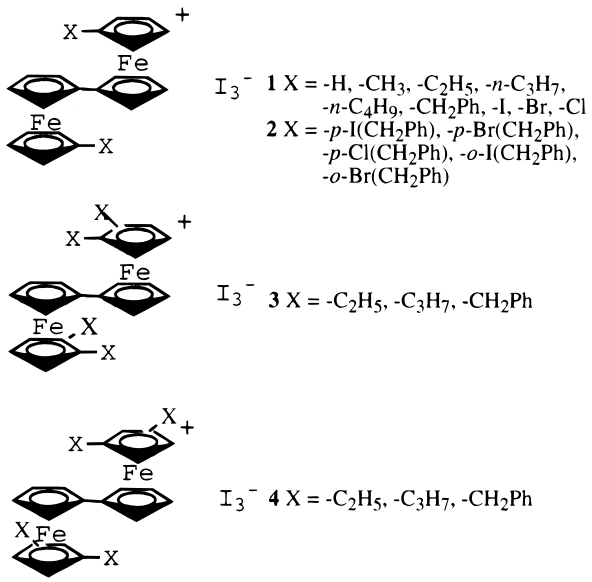

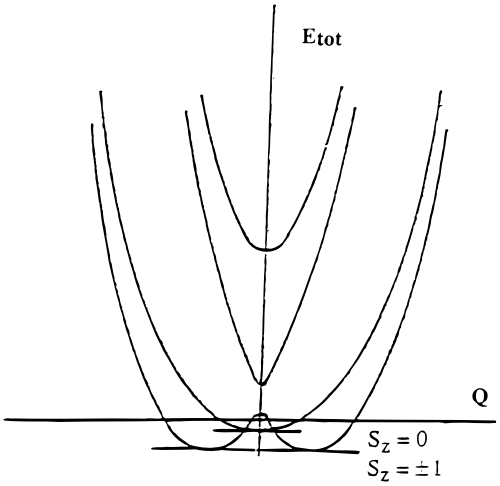

Figure 1. Configurational diagrams. The three-level system that models the molecule is described by a fictitious spin $S = 1$. The pair of levels in the double well is associated with $S_z = \pm 1$; the single level in the single well with $S_z = 0$.

tra. At temperatures below 77 K they each show two doublets, one for the Fe(III) site and the other for the Fe(III) site (electron-transfer rate $< \sim 10^8$ s^{-1}). In each case the two doublets move together with increasing the temperature, eventually, and become a single "average-valence" doublet. Hendrickson suggested[8,9] that the temperature dependence of the Mössbauer spectrum is due to the onset of lattice dynamics associated with the triiodide counterions and alkyl substituents.

Recently, we reported systematic studies of electron transfer in the solid state for a series of mixed-valence biferrocenium cations (**2**−**4**), which have led to a wealth of new experimental results. Major progress has been made in studying the dependence of electron-transfer rates on the lattice dynamics and on the cation−anion interactions, as well as on the structural micromodification. We found that the cation−anion van der Waals interactions between the halide substituent in the benzyl unit and the neighboring triiodide in the series of compounds **2** can have a dramatic influence on the rate of electron transfer.[15] More recently, we prepared a series of polyalkylbiferrocenium triiodide salts (**3**, **4**) to study the influence of ring tilt between two cyclopentadienyl (Cp) rings on electron transfer and to investigate energetic control of electron-transfer rates.[14,22−25] Deviations of the Cp rings from the parallel position were found to correlate quite well with the critical temperature for electronic delocalization−localization in mixed-valence biferrocenium salts.

The quantum-mechanical theory of electronic states of isolated mixed-valence clusters was developed by Tsukerblat.[26] It was shown that the intercluster interaction may lead to the charge-ordered state of the mixed-valence crystal and to interesting peculiarities of the phase transitions. Recently, a Blume−Emery−Griffith (BEG) Hamiltonian was found to provide a qualitative explanation for the various thermal behaviors of electronic localization exhibited by mixed-valence biferrocenium derivative salts in the solid state.[27,28] The BEG Hamiltonian uses a fictitious spin $S = 1$, associated with a three-level system which results from the discretization of the configurational diagram of the biferrocenium cation (Figure 1). Such a particular, triple-well-shaped, diagram is obtained through an extension of the standard PKS model.[29] Most of the Mössbauer data concerning biferrocenium salts could be reproduced by using the $S = 1$ model.

Mixed-valence 1′,1‴-dibenzylbiferrocenium triiodide was reported to have two distinct crystallographic phases which show that the electron-transfer rates are extremely sensitive to changes in crystal lattice.[30] Two different crystalline morphologies (needle and platelike crystals) of 1′,1‴-dibenzylbiferrocenium triiodide were found. The needle crystal in space group $P\bar{1}$ has a Mössbauer spectrum characteric of a valence-detrapped electronic structure down to a temperature of 25 K. The platelike crystal with space group $P2_1/n$ shows a valence-trapped Mössbauer spectrum up to 300 K. However, because of poor diffraction quality and disorder in the triiodide anion, a satisfactory refinement of the structure was not obtained. In our previous communication,[31] we reported the first new mixed-valence compound **5a** (Scheme 1) in two crystallographic phases with satisfactory structural refinements. Our observation is an interesting result that the crystallographic properties of the structure play an important role in controlling the rate of electron transfer. The present work will focus

(21) Kaneko, Y.; Nakano, M.; Sorai, M.; Jang, H. G.; Hendrickson, D. N. *J. Am. Chem. Soc.* **1989**, *28*, 1067.
(22) Dong, T.-Y.; Lee, T. Y.; Lin, H. M. *J. Organomet. Chem.* **1992**, *427*, 101.
(23) Dong, T.-Y.; Chang, C. K.; Huang, C. H.; Wen, Y. S.; Lee, S. L.; Chen, J. A.; Yeh, W. Y.; Yeh, A. *J. Chem. Soc., Chem. Commun.* **1992**, 526.
(24) Dong, T.-Y.; Huang, C. H.; Chang, C. K.; Wen, Y. S.; Lee, S. L.; Chen, J. A.; Yeh, W. Y.; Yeh, A. *J. Am. Chem. Soc.* **1993**, *115*, 6357.
(25) Dong, T.-Y.; Lee, S. H.; Chang, C. K.; Lin, H. M.; Lin, K. J. *Organometallics* **1997**, *16*, 2773.
(26) Koryachenko, A. V.; Klokishner, S. I.; Tsukerbat, B. S. *Chem. Phys.* **1991**, *150*, 295.
(27) Boukheddaden, K.; Linares, J.; Galam, S.; Varret, F. *J. Phys.: Condens. Matter* **1993**, *5*, 1.
(28) Boukheddaden, K.; Linares, J.; Galam, S.; Varret, F. *J. Phys.: Condens. Matter* **1993**, *5*, 5179.
(29) Wong, K. Y.; Schatz, P. N. *Prog. Inorg. Chem.* **1981**, *28*, 369.
(30) Webb, R. J.; Dong, T.-Y.; Pierpont, C. G.; Boone, S. R.; Chadha, R. K.; Hendrickson, D. N. *J. Am. Chem. Soc.* **1991**, *113*, 4806.
(31) Dong, T.-Y.; Lai, X. Q.; Lin, K. J. *Angew. Chem., Int. Ed. Engl.* **1997**, *36*, 2002.

Scheme 1

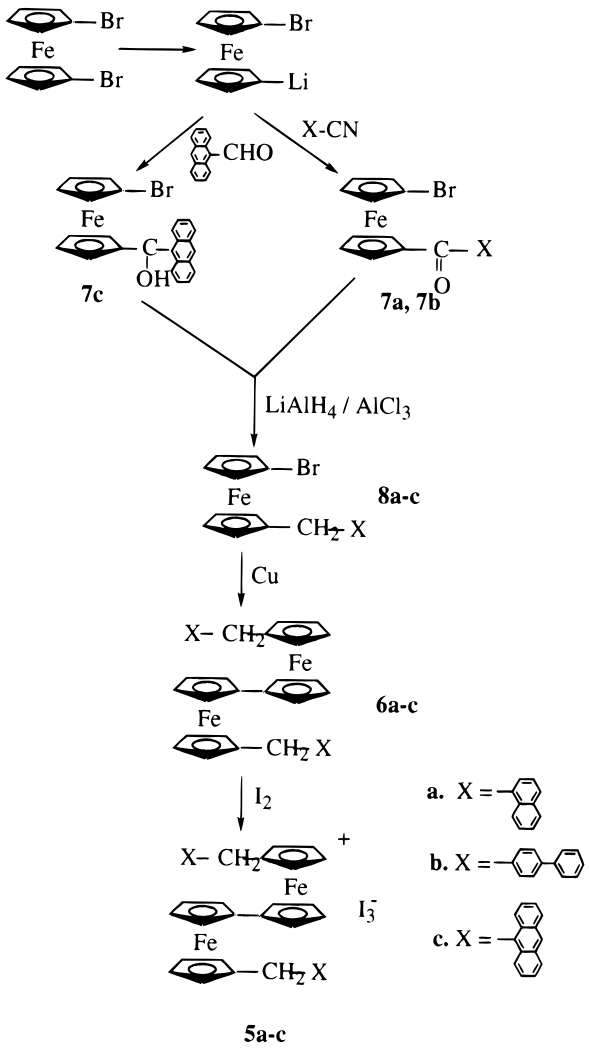

on the spectroscopic measurements for mixed-valence cations **5a**−**c**. The understanding of electron-transfer processes in **5a**−**c** provides detailed insight into the fundamental theoretic aspect of charge ordering and phase transitions in molecular crystals. Thus the general importance of this study is that it is a test case for the cooperative $S = 1$ model. The results of the X-ray structural work on **5a**,**b** together with the electrochemical measurements, variable-temperature Mössbauer data, and EPR measurements are presented in this paper.

Results and Discussion

Molecular Structure of Neutral Biferrocene 6a. Details of the X-ray crystal data collections and unit-cell parameters are given in Table 1. The molecular structure of **6a** is shown in Figure 2, and selected bond distances and angles are given in Table 2. This neutral biferrocene exists in a trans conformation with the two iron ions on opposite sides of the planar fulvalenide bridge.

In **6a**, the average distance from the Fe ion to the C atoms is 2.042(4) Å. Furthermore, there is no significant difference between the Fe−Cp distance (1.650(6) Å) and Fe−fulvalenide distance (1.649(1) Å). Inspection of the Fe−Cp distances shows that these values are closer to

Table 1. Experimental and Crystal Data for the X-ray Structures of 5a and 6a

	5a	5a	6a
formula	$C_{42}H_{34}Fe_2I_3$	$C_{42}H_{34}Fe_2I_3$	$C_{42}H_{34}Fe_2$
mw	1031.1	1031.1	650.40
cryst syst	triclinic	monoclinic	triclinic
space group	$P\bar{1}$	$P2_1/n$	$P\bar{1}$
a, Å	9.836(2)	17.286(5)	8.229(2)
b, Å	10.418(2)	9.188(7)	8.477(2)
c, Å	10.638(3)	23.069(4)	11.202(3)
α, deg	62.83(1)		91.45(1)
β, deg	86.06(1)	93.44(2)	103.99(1)
γ, deg	69.74(1)		95.74(1)
V, Å^3	904.5(4)	3658(3)	753.4(3)
Z	1	4	1
D_{calcd}, g cm^{-3}	1.893	1.873	1.433
μ, mm^{-1}	3.391	3.355	0.993
λ, Å	0.70930	0.70930	0.70930
θ limits, deg	22.42	22.43	22.42
R1	0.0354	0.0348	0.0260
wR(f^2)	0.0875	0.0980	0.0703

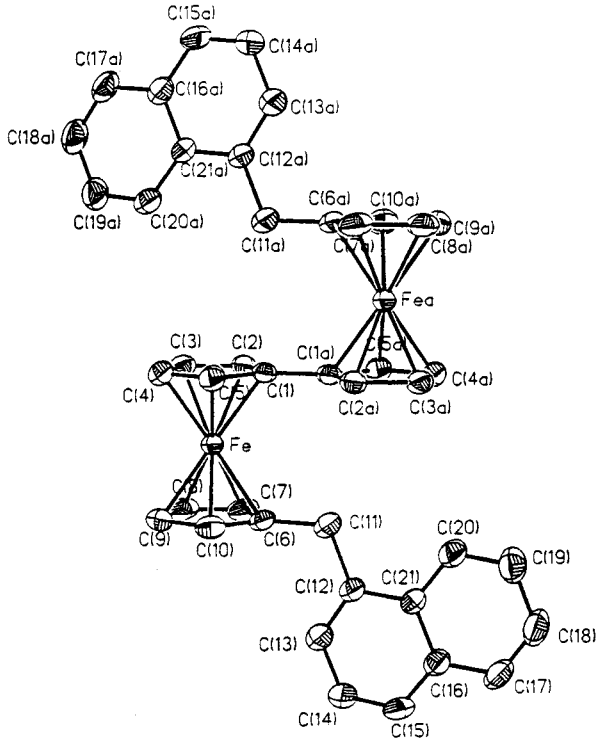

Figure 2. ORTEP drawing for **6a** with 50% thermal ellipsoids.

the value of 1.65 Å found for ferrocene[32] than to the value of 1.70 Å found for the ferrocenium ion.[33] The dihedral angle between the two least-squares planes of the Cp rings for the ferrocenyl moiety in **6a** is 1.0°, while the two Cp rings bonded to the iron ion are nearly eclipsed, with average staggering angle of 1.2°.

Molecular Structure of 5a. 1′,1‴-Dinaphthylmethylbiferrocenium triiodide (**5a**) exhibits two crystalline morphologies at room temperature. Dark crystals in the triclinic space group $P\bar{1}$ were formed when a CH_2Cl_2 solution of **5a** was allowed to evaporate slowly. The refinement of the structure imposed inversion centers on both the cation and the triiodide anion. Thus, the two ferrocenyl moieties are crystallographically equiva-

(32) Seiler, P.; Dunitz, J. D. *Acta Crystallogr., Sect. B* **1979**, *35*, 1068.
(33) Mammano, N. J.; Zalkin, A.; Landers, A.; Rheingold, A. L. *Inorg. Chem.* **1977**, *16*, 297.

Table 2. Selected Bond Distances (Å) and Angles (deg) of 5a and 6a

	6a	5a[a]	5a[b]
Fe−C(1)	2.060(2)	2.090(5)	
Fe−C(2)	2.040(2)	2.055(6)	
Fe−C(3)	2.038(3)	2.039(6)	
Fe−C(4)	2.040(2)	2.046(6)	
Fe−C(5)	2.042(2)	2.050(6)	
Fe−C(6)	2.052(2)	2.074(5)	
Fe−C(7)	2.037(3)	2.043(5)	
Fe−C(8)	2.034(3)	2.053(6)	
Fe−C(9)	2.039(3)	2.064(6)	
Fe−C(10)	2.034(3)	2.073(6)	
Fe(1)−C(1)			2.053(6)
Fe(1)−C(2)			2.054(7)
Fe(1)−C(3)			2.067(7)
Fe(1)−C(4)			2.056(7)
Fe(1)−C(5)			2.028(7)
Fe(1)−C(6)			2.065(6)
Fe(1)−C(7)			2.046(6)
Fe(1)−C(8)			2.043(6)
Fe(1)−C(9)			2.055(6)
Fe(1)−C(10)			2.043(6)
Fe(2)−C(11)			2.129(6)
Fe(2)−C(12)			2.095(7)
Fe(2)−C(13)			2.047(7)
Fe(2)−C(14)			2.050(7)
Fe(2)−C(15)			2.079(9)
Fe(2)−C(16)			2.126(7)
Fe(2)−C(17)			2.091(7)
Fe(2)−C(19)			2.069(7)
Fe(2)−C(20)			2.110(7)
I(1)−I(2)		2.8936(8)	2.8950(11)
I(3)−I(1)			2.9318(10)
I(2)−I(1)−I(2)[c]		180.0	
I(2)−I(1)−I(3)			176.31(2)

[a] With $P\bar{1}$ phase. [b] With $P2_1/n$ phase. [c] Symmetry equivalents: $-x, -y, -z$.

lent. An ORTEP plot of the molecular structure is given in Figure 3a, whereas Figure 4a shows an extended packing arrangement adopted in this $P\bar{1}$ phase. Collected in Table 2 are selected bond distances and angles.

Inspection of the iron to Cp ligand bond lengths (Fe−Cp, 1.668(2) and 1.676(2) Å) shows that both distances are intermediate between the analogous values for neutral ferrocene (1.65 Å)[32] and the ferrocenium ion (1.70 Å).[33] The average Fe−C distance is 2.059(5) Å, which is also intermediate between the value for ferrocene (2.045(1) Å) and the ferrocenium ion (2.075 Å). The plane of the Cp ring forms a dihedral angle of 4.4° with the fulvalenide plane, and the two Cp rings in each ferrocenyl moiety are not perfectly eclipsed but are rotated relative to one another by 7.0°. As shown in Figure 4a, an intermolecular naphthyl−naphthyl ($\pi-\pi$) interaction (3.648 Å) is observed between neighbor cations. We believe that this $\pi-\pi$ interaction plays a quite important role in controlling the intramolecular electron-transfer rate. A detailed discussion will be presented in the last section.

In $P\bar{1}$ phase, the I_3^- anion is at the inversion center, showing a symmetric structure. The I−I bond distance is 2.8936(8) Å, which compares well with other determinations of the symmetric triiodide bond distance.[34] The triiodide is strictly linear as required by the inversion symmetry.

Dark crystals in the monoclinic space group $P2_1/n$ were obtained when a layer of hexane was allowed to slowly diffuse into a CH_2Cl_2 solution of **5a**. The molecular structure is also shown in Figure 3b, whereas Figure 4b shows a packing arrangement adopted in this $P2_1/n$ phase. Collected in Table 2 are given selected bond distances and angles for this structure.

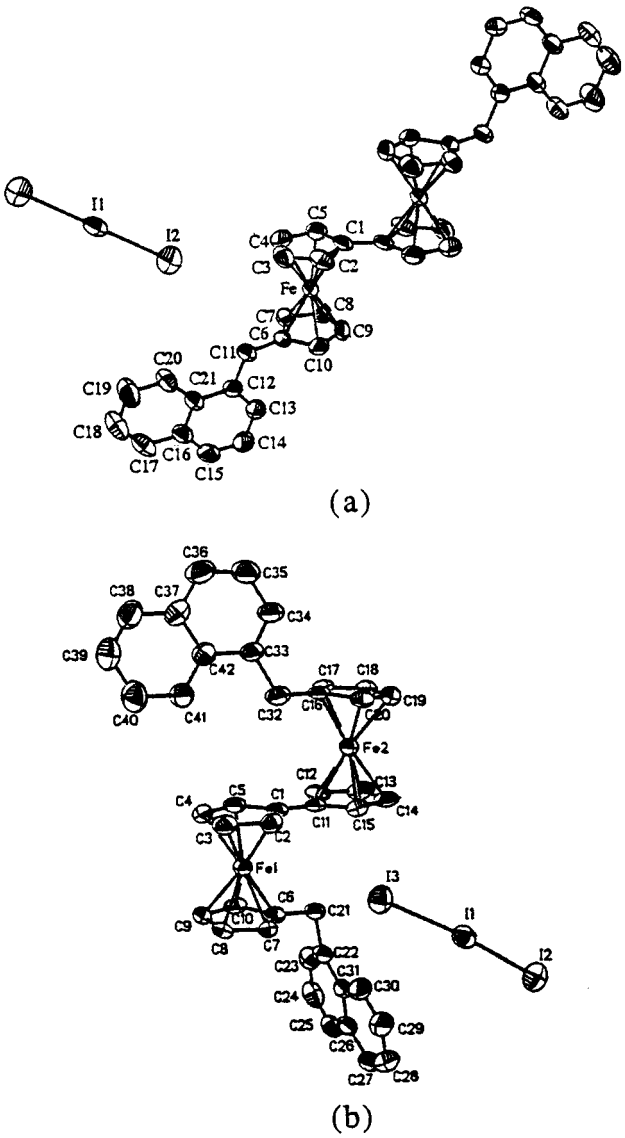

Figure 3. (a) ORTEP drawing for **5a** with $P\bar{1}$ phase obtained when a CH_2Cl_2 solution of **5a** was allowed to evaporate slowly. (b) ORTEP drawing for **5a** with $P2_1/n$ phase obtained when a layer of hexane was allowed to slowly diffuse into a CH_2Cl_2 solution of **5a**.

In $P2_1/n$ phase, the two metallocene moieties in the cation are not equivalent. The average Fe1−C distance (2.052(4) Å) and the Fe1−Cp distance (1.660(4) Å) indicate that this metallocene is in the Fe(II) oxidation state. In contrast, the average Fe2−C distance (2.086(5) Å) and average Fe2−Cp distance (1.693(4) Å) indicate that this metallocene is in the Fe(III) oxidation state. The two Cp rings associated with Fe1 and Fe2 are not quite parallel, and the dihedral angles are 2.1° and 5.5°, respectively. Furthermore, the two Cp rings associated with Fe1 and Fe2 are nearly eclipsed, with average staggering angles of 3.0° and 2.3°, respectively. The extended packing arrangement of the $P2_1/n$ phase of **5a** consists of columns of interacting cations surrounded by triiodide anions (Figure 4b). The closest cation−

(34) Runsink, J.; Swen-Walstra, S.; Migchelsen, T. *Acta Crystallogr. B* **1972**, *28*, 1331.

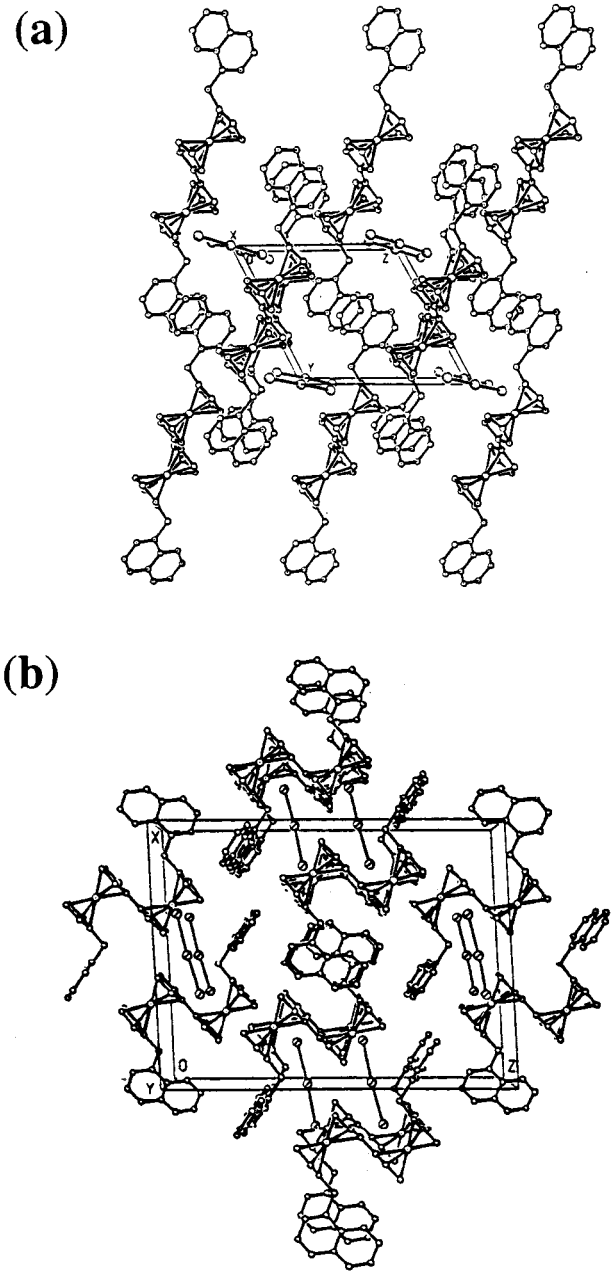

Figure 4. (a) Packing arrangement of **5a** with $P\bar{1}$ phase. (b) Packing arrangement of **5a** with $P2_1/n$ phase.

cation contacts result from intermolecular contacts of naphthyl substituents. However, the naphthyl rings in the $P2_1/n$ phase of **5a** are not anywhere to contact to each other, as found in the $P\bar{1}$ phase of **5a**. Only the naphthyl substituent associated with the Fe(III) metallocene and the naphthyl substituent on another Fe(III) metallocene in another cation column contact each other. They contact in a parallel edge-to-edge fashion such that the shortest cation−cation contact is 3.789 Å.

In the case of the $P2_1/n$ phase, the triiodide anion is asymmetric (I1−I2 2.895(1), I1−I3 2.932(1) Å). In other words, the I3 atom carries more negative charge, showing I2−I1····$I3^-$ character. Furthermore, the $I3^-$ anion is not quite linear (176.31(2)°).

A comparison of structural features between the two different crystallographic phases of **5a** is interesting. The naphthylmethyl substituent on the Cp ring is situated differently. The two nonequivalent naphthylmethyl substituents in the cation with $P2_1/n$ phase show a cisoid conformation relative to the fulvalenide ligand, and this is similar to other dialkyl mixed-valence biferrocenium triiodide salts. In the case of the cation with $P\bar{1}$ phase, the two equivalent naphthylmethyl substituents show a transoid conformation relative to the fulvalenide ligand. Consequently, the packing arrangement of the cations and anions of **5a** with $P2_1/n$ phase is different from that with $P\bar{1}$ phase. The packing arrangement for both phases can be described as columns of cations and anions. However, it appears the naphthylmethyl substituents with $P2_1/n$ phase lead to further slippage of the cations from the steplike stacks seen in the $P\bar{1}$ phase.

Table 3. Cyclic Voltammetry for Various Biferrocenes

compound	$E_{1/2}$(V)[a]	$\Delta E_{1/2}$(V)[b]	Δ (mV)[c]	$10-5 \times K_{com}$[d]
biferrocene	0.31	0.31	70	1.80
	0.62		75	
6a	0.33	0.35	61	8.6
	0.68		60	
6b	0.32	0.35	73	8.6
	0.67		58	
6c	0.33	0.34	63	5.8
	0.67		60	

[a] All half-wave potentials are referred to the AgCl/Ag electrode. [b] Peak separation between two waves. [c] Peak-to-peak separation between the resolved reduction and oxidation wave maxima. [d] K_{com}: comproportionation equilibrium constants.

Electrochemical Results. Electrochemical data for neutral biferrocenes **6a**−**c**, as well as those for some other relevant compounds, are shown in Table 3. These binuclear biferrocenes all show two successive reversible one-electron oxidation−reduction waves. Electrochemical reversibility was demonstrated by the peak-to-peak separation between the resolved reduction and oxidation wave maxima and a 1:1 relationship of the cathodic and anodic peak currents.

In comparison with biferrocene, the substituents on the Cp rings in **6a**−**c** clearly act as net electron-withdrawing groups. It has been reported that the peak-to-peak ($\Delta E_{1/2}$) separation can gauge the interaction between the two Fe sites in a biferrocenium cation.[35,36] The separations between the two oxidation−reduction waves for **6a**−**c** are 0.35, 0.35, and 0.34 V, respectively. In other words, the magnitudes of the electronic interactions between the two Fe sites in **5a**−**c** are nearly equivalent in solution state.

^{57}Fe Mössbauer Characteristics. It has been noted that the ^{57}Fe Mössbauer spectral properties of 1′,1‴-dialkylbiferrocenium triiodide salts are dependent on sample history.[8−12] To examine this phenomenon more thoroughly, we prepared samples of **5a**−**c** by three different methods as described in the Experimental Section. First, we examined a microcrystalline sample of **5a**, formed by adding a benzene solution of iodine to a benzene solution of corresponding neutral biferrocene

(35) Morrison, W. H., Jr.; Krogsrud, S.; Hendrickson, D. N. *Inorg. Chem.* **1973**, *12*, 1998.

(36) (a) Atzkern, H.; Huber, B.; Köhler, F. H.; Müller, G.; Müller, R. *Organometallics* **1991**, *10*, 238. (b) Bunel, E. E.; Campos, P.; Ruz, P.; Valle, L.; Chadwick, I.; Ana, M. S.; Gonzalez, G.; Manriquez, J. M. *Organometallics* **1988**, *7*, 474. (c) Cowan, D. O.; Shu, P.; Hedberg, F. L.; Rossi, M.; Kistenmacher, T. J. *J. Am. Chem. Soc.* **1979**, *101*, 1304. (d) Moulton, R.; Weidman, T. W.; Vollhardt, K. P. C.; Bard, A. *J. Inorg. Chem.* **1986**, *25*, 1846. (e) Obendorf, D.; Schottenberger, H.; Rieker, C. *Organometallics* **1991**, *10*, 1293.

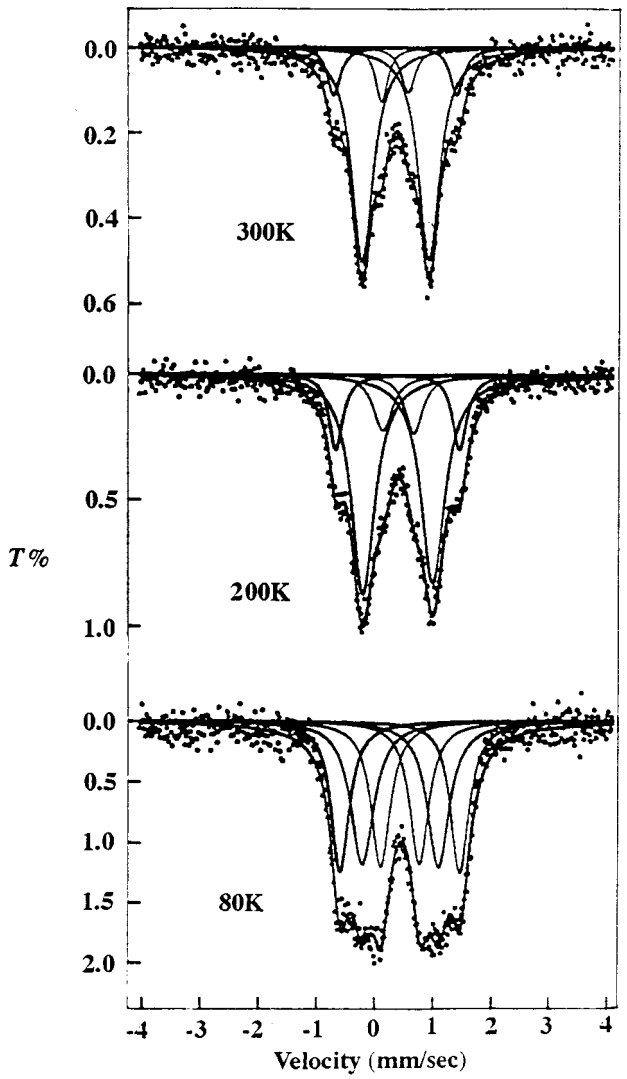

Figure 5. Variable-temperature ^{57}Fe Mössbauer spectra of **5a** prepared by method 1.

6a (method 1). The variable-temperature ^{57}Fe Mössbauer spectra are shown in Figure 5. The various absorption peaks were fitted to Lorentzian lines. The resulting fitting parameters are collected in Table 4. The prominent features in the 80 K Mössbauer spectrum are two doublets, one with a $\Delta E_Q = 2.063$ mms^{-1} (Fe(II) metallocene) and the other with a $\Delta E_Q = 0.653$ mms^{-1} (Fe(III) metallocene). Both doublets were fitted to have the same area. This pattern of two doublets is what is expected for a mixed-valence biferrocenium cation which is valence trapped on the Mössbauer time scale ($\sim 10^8$ s^{-1}). Fitting the 80 K spectrum also clearly shows a third doublet with $\Delta E_Q = 1.318$ mms^{-1}. This doublet is associated with a mixed-valence biferrocenium cation in which the electron-transfer rate is greater than the Mössbauer time scale. The ratio of valence-localized to valence-delocalized species in the 80 K spectrum is 1.67:1.00. As the temperature is increased, the intensity of the detrapped signal grows at the expense of trapped signal. The ratio of valence-localized to valence-delocalized species charges from 1.67:1.00 to 1.00:3.50 as the temperature is changed from 80 to 300 K.

The observations of the structural characteristics of **5a** are also consistent with our Mössbauer studies. ^{57}Fe Mössbauer spectra for a more crystalline sample of **5a** with the $P\bar{1}$ phase, prepared by slow evaporation from a CH_2Cl_2 solution (method 2), were also collected at temperatures ranging from 80 to 300 K. Selected spectra are shown in Figure 6, and the fitting parameters are listed in Table 4. At temperatures below 100 K, the cation of **5a** shows two doublets in the variable-temperature Mössbauer spectra, one representing the Fe(II) site and the other for the Fe(III) site. An increase of temperature causes the two doublets to move together, resulting in an "average-valence" doublet at 130 K. At 300 K, the spectrum of this sample shows a single doublet which is characteristic of a valence-detrapped cation in which the electron-transfer rate exceeds $\sim 10^8$ s^{-1}.

On the other hand, the sample of **5a** with $P2_1/n$ phase, prepared by slowly diffusing hexane into a CH_2Cl_2 solution containing **5a** (method 3), exhibits a Mössbauer spectrum characteric of a valence-trapped cation (Fe(II),

Table 4. ^{57}Fe Mössbauer Least-Squares-Fitting Parameters

compound	T, K	ΔE_Q[a]	δ[b]	Γ[c]	area ratio[d]
5a[e]	300	0.438	0.438	0.296, 0.247	1.00:3.50
		1.129	0.447	0.448, 0.442	
		2.077	0.441	0.282, 0.282	
	200	0.523	0.511	0.373, 0.391	1.00:2.39
		1.207	0.505	0.502, 0.476	
		2.127	0.502	0.292, 0.291	
	80	0.653	0.540	0.397, 0.389	1.67:1.00
		1.318	0.539	0.465, 0.474	
		2.063	0.538	0.374, 0.377	
5a[f]	300	1.120	0.451	0.427, 0.441	
	250	1.138	0.472	0.463, 0.467	
	150	1.223	0.525	0.576, 0.590	
	140	1.206	0.519	0.586, 0.604	
	130	1.242	0.532	0.596, 0.650	
	120	0.956	0.537	0.496, 0.453	
		1.539	0.524	0.486, 0.472	
	110	0.902	0.523	0.459, 0.459	
		1.516	0.516	0.456, 0.511	
	80	0.818	0.528	0.543, 0.498	
		1.610	0.516	0.502, 0.511	
5a[g]	300	0.407	0.430	0.285, 0.281	
		2.085	0.441	0.251, 0.267	
5b[e]	300	0.543	0.421	0.501, 0.445	
		1.906	0.434	0.337, 0.361	
5b[f]	300	0.501	0.416	0.457, 0.457	
		1.842	0.427	0.350, 0.350	
	80	0.634	0.532	0.418, 0.403	
		2.062	0.523	0.264, 0.270	
5b[g]	300	0.337	0.416	0.330, 0.330	2.00:1.00
		0.782	0.411	0.402, 0.404	
		2.079	0.462	0.358, 0.335	
	80	0.357	0.516	0.395, 0.395	3.57:1.00
		1.134	0.503	0.552, 0.552	
		2.099	0.524	0.307, 0.307	
5c[e]	300	1.156	0.453	0.395, 0.402	
	150	1.222	0.512	0.530, 0.526	
	120	1.239	0.521	0.598, 0.604	
	110	0.992	0.534	0.485, 0.462	
		1.544	0.518	0.581, 0.545	
	100	0.975	0.529	0.479, 0.479	
		1.628	0.525	0.493, 0.523	
	90	0.916	0.534	0.487, 0.455	
		1.665	0.518	0.514, 0.513	
	80	0.866	0.532	0.479, 0.453	
		1.7231	0.520	0.472, 0.480	

[a] Quadrupole-splitting in mms^{-1}. [b] Isomer shift referenced to iron-foil in mms^{-1}. [c] Full width at half-height taken from the least-squares-fitting program. The width for the line at more positive velocity is listed first for each doublet. [d] The ratio of localized state to delocalized state. [e] Microcrystalline sample. [f] Prepared by evaporating the CH_2Cl_2 solution of biferrocenium. [g] Prepared by diffusing the hexane into the CH_2Cl_2 solution of biferrocenium.

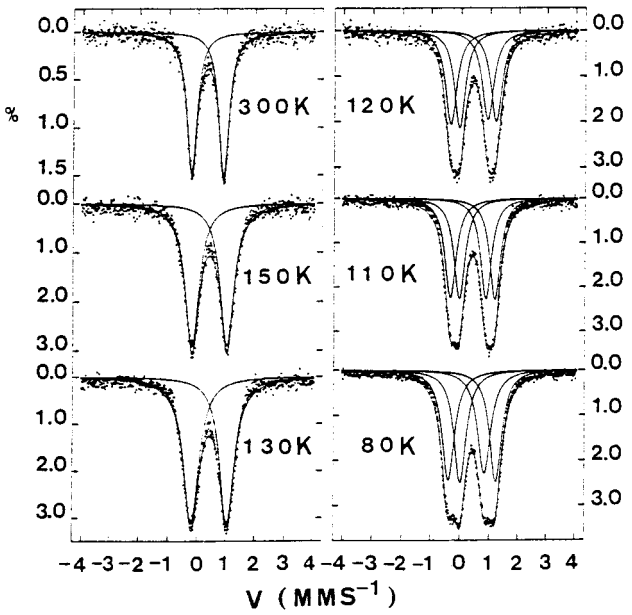

Figure 6. Variable-temperature ^{57}Fe Mössbauer spectra of **5a** with $P\bar{1}$ phase prepared by method 2.

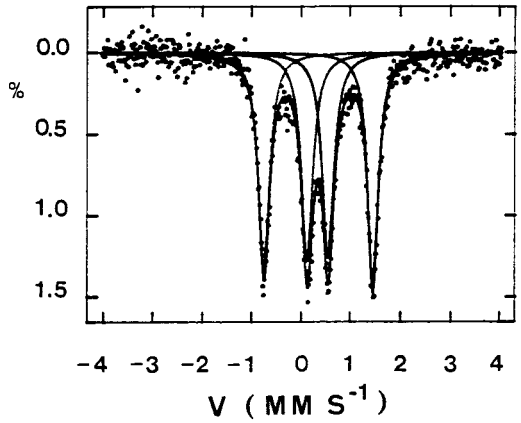

Figure 7. Variable-temperature ^{57}Fe Mössbauer spectra of **5a** with $P2_1/n$ phase prepared by method 3.

ΔE_Q = 2.085 mms^{-1}; Fe(III), ΔE_Q = 0.407 mms^{-1}), which remains trapped even at 300 K (Figure 7). Obviously, the intramolecular electron transfer in **5a** is quite sensitive to environmental perturbations caused by different crystal-packing arrangements.

Three different preparations of **5b** were also examined with variable-temperature Mössbauer spectroscopy. Figure 8 illustrates the spectra obtained for samples prepared by methods 1 and 2. The features in all these spectra include two doublets, one with a $\Delta E_Q = \sim 2$ mms^{-1} (Fe(II) site) and the other with $\Delta E_Q = \sim 0.5$ mms^{-1} (Fe(III) site). Both doublets have the same area. This pattern of two doublets is expected for a mixed-valence biferrocenium cation which is valence-trapped on the time scale of the Mössbauer technique (electron-transfer rate $< \sim 10^8$ s^{-1} on the solid state). The sample of **5b** obtained by method 3 gives Mössbauer spectra with localized (two doublets) and delocalized (one average doublet) spectra superimposed. Collected in Table 4 are the resulting fitting parameters.

Owing to the low solubility of **5c** in the CH_2Cl_2 solvent, we could not study the dependency of sample history. However, ^{57}Fe Mössbauer spectra for a sample

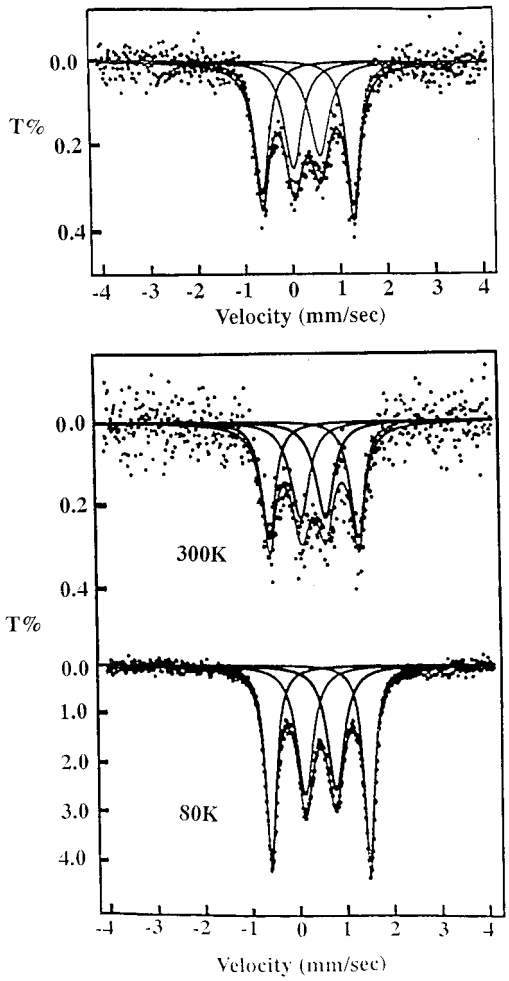

Figure 8. Variable-temperature ^{57}Fe Mössbauer spectra of **5b** prepared by methods 1 (top) and 2 (bottom).

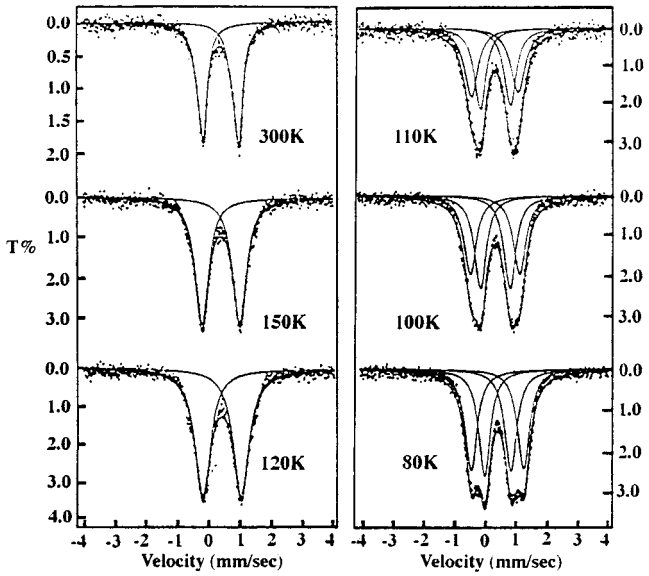

Figure 9. Variable-temperature ^{57}Fe Mössbauer spectra of **5c** prepared by method 1.

of **5c** obtained by method 1 were also collected at temperatures ranging from 80 to 300 K. Selected spectra are shown in Figure 9, and the fitting parameters are listed in Table 4. At temperatures below 110 K, the cation of **5c** shows two doublets (electron-transfer rate $< \sim 10^8$ s^{-1}). The two doublets are seen to move together

as the sample temperature is increased, finally becoming a single average doublet at ~120 K.

Our Mössbauer results indicate that changing the substituent in the biferrocenium cations **5a**−**c** leads to dramatic changes in the electron-transfer rate in the solid state. The interactions of the cation−cation and the cation−anion undoubtedly alter the structural packing arrangement and therefore the potential energy surface of the mixed-valence molecule. We believe that the difference in electron-transfer rate is not due to a difference in the electronic effect of the substituents. The electrochemical measurements for the corresponding neutral biferrocenes **6a**−**c** strongly support our suggestion. In the last section, we will provide an explanation for the difference in electron-transfer rates in the mixed-valence cations **5a**−**c**.

Electron Paramagnetic Resonance. For a mononuclear ferrocenium cation with no low-symmetry crystal field distortion, an axial-type spectrum will be observed with $g_{\parallel} = 6$ and $g_{\perp} = 0$. As the low-symmetry crystal field increases, both $g_{\parallel}$ and $g_{\perp}$ approach a value of 2. In the case of a binuclear mixed-valence biferrocenium cation, the value of the g tensor anisotropy (Δg) can be used as a rough estimate of the nature of the electronic ground state of the mixed-valence biferrocenium cation. Hendrickson reported that systems with larger g tensor anisotropy ($\Delta g > 1.5$) are valence trapped on the Mössbauer time scale at all temperatures, while those with small anisotropy ($\Delta g < 1.1$) are valence detrapped throughout the thermally accessible temperature range.[30] Systems with Δg between 1.1 and 1.5 show Mössbauer behavior intermediate between these two extremes; they are valence trapped at low temperatures and can become detrapped at higher temperatures. Here, we are interested in studying the nature of the electronic ground state of the two different crystalline morphologies of mixed-valence cation **5a** by EPR technique.

X-band EPR spectra were run for the samples of **5a** with $P\bar{1}$ phase and $P2_1/n$ phase at 77 K. Spectra are shown in Figure 10, and the g values evaluated from these spectra and other related EPR spectra are collected in Table 5. The 77 K spectrum of **5a** with $P\bar{1}$ phase is clearly a typical axial-type spectrum ($g_{\parallel} = 3.16$ and $g_{\perp} = 1.91$). Surprisingly, the 77 K spectrum of **5a** with $P2_1/n$ phase consists of two $g_{\parallel}$ signals (3.67 and 2.85) and two $g_{\perp}$ signals (2.01 and 1.79). Furthermore, it seems that the $g_{\parallel}$ value of 3.16 for the $P\bar{1}$ phase lies midway between the $g_{\parallel}$ values of 3.67 and 2.85 for the $P2_1/n$ phase. Similarly, the feature at $g_{\perp} = 1.91$ for the $P\bar{1}$ phase lies midway between the features at $g_{\perp} = 2.01$ and 1.79 for the $P2_1/n$ phase. To explain this unusual observation at 77 K, we cannot simply conclude that the sample of **5a** with $P\bar{1}$ phase exhibits a delocalized EPR spectrum (electron-transfer rate > $\sim 10^{10}$ s^{-1}) and the sample of **5a** with $P2_1/n$ phase exhibits a localized EPR spectrum. At 77 K, our Mössbauer results indicate that the intramolecular electron-transfer rates are less than the time scale ($\sim 10^8$ s^{-1}) of Mössbauer technique for both phases. This observation can be interpreted in terms of the $S = 1$ model.

As mentioned in the introduction, the $S = 1$ model is a theory of charge ordering and phase transition in molecular crystals. This model involves intramolecular

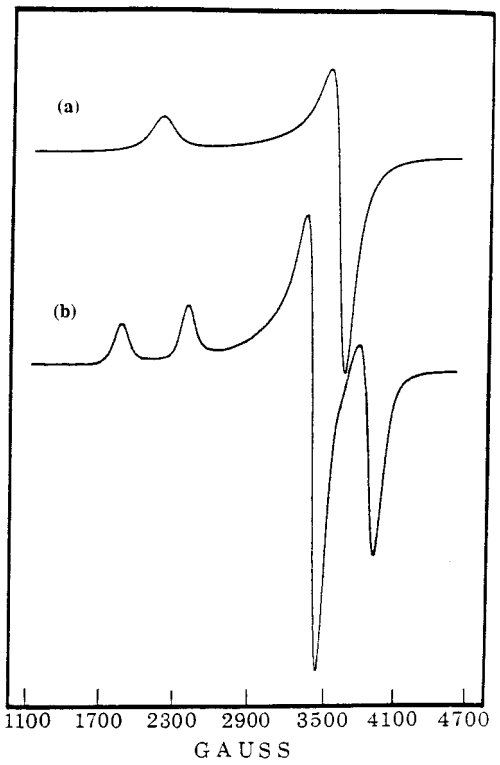

Figure 10. EPR spectra of **5a** (a) with $P\bar{1}$ phase and (b) with $P2_1/n$ phase.

Table 5. EPR Data of 5a and Other Related Compounds

compound[a]	T/K	$g_{\parallel}$	$g_{\perp}$	Δg[b]
biferrocenium I_3[c]	4.2	3.58	1.72	1.86
1′,1‴-dibutylbiferrocenium I_3[c]	4.2	2.98	1.92	1.06
1′,1‴-dibenzylbiferrocenium I_3[c]	4.2	3.02	2.01	1.07
			1.89	
1′,1‴-diiodobiferrocenium I_3[c]	4.2	2.75	2.01	0.76
			1.97	
5a[d]	77	3.16	1.91	1.25
5a[e]	77	3.67	2.01	1.66
		2.85	1.79	1.06

[a] Powder sample. [b] $\Delta g = g_{\parallel} - g_{\perp}$. [c] From ref 29. [d] With $P\bar{1}$ phase. [e] With $P2_1/n$ phase.

Heisenberg-type exchange interaction, as well as dipole−dipole intermolecular interaction. It was found to provide a qualitative explanation for the various thermal behaviors of electronic localization exhibited by mixed-valence biferrocenium salts in the solid state. As shown in Figure 1, the three-level system is described by a fictitious spin $S = 1$. The pair of levels in the double well is associated with $s_z = \pm 1$ and the single level in the single well with $s_z = 0$ and a 2-fold degeneracy. The levels of $S_z = 0, \pm 1$ can be considered respectively as "delocalized" and "localized" states. This model suggests a coexistence of localized and delocalized components with progressive conversion. In terms of the $S = 1$ model, we would like to suggest that the origin for our usual EPR observation of **5a** with $P2_1/n$ phase arises from the interaction of spin−spin exchange resulting from a dipole−dipole interaction which develops between trapped cations. Therefore, in an effort to assess the evidence for spin−spin interactions in **5a**, the solid-state packing arrangements of both phases are examined in detail. The closest Fe−Fe contacts in **5a** appear in Figure 11. The packing arrangements are displayed

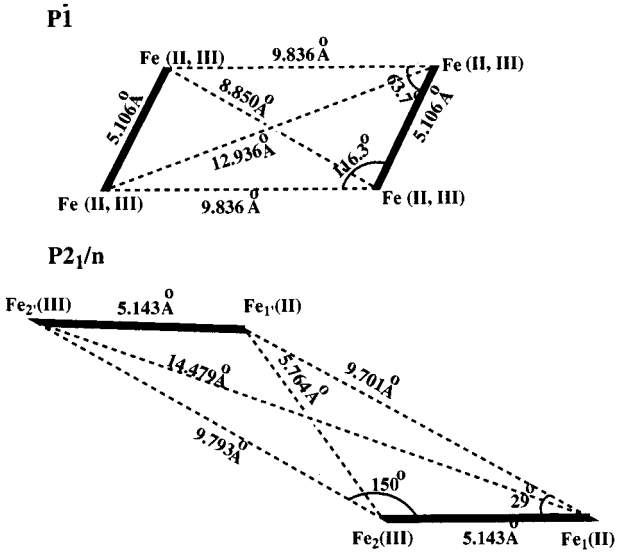

Figure 11. Geometry of the closest intermolecular contacts between cations of **5a** with (a) $P\bar{1}$ phase and (b) $P2_1/n$ phase.

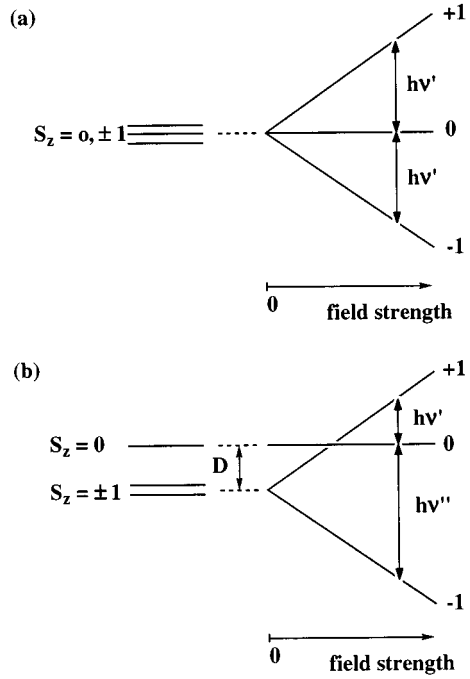

Figure 12. Zero-field and magnetic field splitting of energy levels.

in Figure 4. The $P\bar{1}$ phase of **5a** results in cation−cation interactions throughout the cation column generated by the inversion center. Furthermore, this Fe−Fe contacting in the $P\bar{1}$ phase occurs with parallelogram fashion. In the $P\bar{1}$ phase, the two ferrocenyl moieties in each cation are crystallographically equivalent. Thus, the unpaired electron in e_{2g} ($d_{x^2-y^2}$, d_{xy}) orbitals can oscillate back and forth between the two Fe centers in each biferrocenium cation. In contrast to the $P\bar{1}$ phase, the unpaired electron in the biferrocenium cation with $P2_1/n$ phase is located primarily in the Fe(III) center, since the two ferrocenyl moieties are not crystallographically equivalent. The $P2_1/n$ crystal structure of **5a** results in pairwise cation−cation contact. The closest Fe(III)−Fe(III) contact in the $P2_1/n$ phase is 9.793 Å. A stronger dipole−dipole interaction in the $P2_1/n$ phase can be expected to produce a singlet−triplet splitting (Figure 12, $D_{\|} = 540$ G, $D_{\perp} = 450$ G). This explains why two $g_{\|}$ and two $g_{\perp}$ signals were observed in the EPR spectrum of **5a** with $P2_1/n$ phase.

Concluding Comments. The goal of this section is to present an explanation for the differences of electron-transfer rates in the series of mixed-valence biferrocenium cations.

To explain the dependence of sample history of Mössbauer results, Hendrickson suggested[37] that the factors that are potentially important in controlling the rate of intramolecular electron transfer in a mixed-valence cation include (1) the effective barrier for electron transfer in the cation, (2) the effective barrier for charge oscillation in the anion, and (3) the intermolecular cation−cation and cation−anion interactions. A change in valence for a transition metal complex is generally accompanied by a sizable coordination sphere reorganization. For an iron metallocene, the distance between Fe and Cp ring centroid changes from 1.65 Å for Fe(II) to 1.70 Å for Fe(III). When an intramolecular electron transfer occurs in a biferrocenium cation, the two Cp rings bound to the Fe(II) ion move away from the metal to adjust their distance to the larger dimension appropriate for a $(Cp)_2Fe(III)$ moiety. At the same time the dimensions of the $(Cp)_2Fe(III)$ moiety contract to those of a $(Cp)_2Fe(II)$ species. In Hendrickson's model, the 3d electrons of the Fe ions couple strongly with this out-of-phase combination of Cp−Fe−Cp breathing modes. Recently, we also suggested that the Cp ring tilting must be considered in the Hendrickson micromodulation picture.[22−25] Furthermore, the theoretical $S = 1$ model supports the coexistence of localized and delocalized states.[27,28]

Hendrickson's model can be applied to explain the absence of line broadening observed in the variable-temperature Mössbauer spectra of **5a** with $P\bar{1}$ phase. The observed changes in Mössbauer spectra are attributable to the onset of lattice dynamics in the $P\bar{1}$ phase occurring at a rate that is fast on the Mössbauer time scale at all temperatures.

The differences in the ^{57}Fe Mössbauer spectral properties between two phases can be attributable to the differences in the molecular conformation of the biferrocenium cation. In the $P\bar{1}$ phase, the crystal structure results show that the two ferrocenyl moieties of the cation are symmetric. Rapid electron transfer is then possible in this symmetric arrangement. The cations with $P2_1/n$ phase are asymmetric; that is, the two irons are not in equivalent environments. This asymmetry results in a zero-point energy difference for intramolecular electron transfer. On the basis of the $S = 1$ model, the zero-point energy difference between two vibronic states for a biferrocenium cation is proportional to the cation−cation interaction. As mentioned in the section on EPR, the cations in the $P2_1/n$ phase exhibit stronger cation−cation (dipole−dipole) interactions. Thus, one vibronic state of the mixed-valence cation is energetically more stable than the other state. This explains why a localized electronic structure of **5a** with $P2_1/n$ phase was observed.

(37) Kambara, T.; Hendrickson, D. N.; Dong, T.-Y.; Cohn, M. J. *J. Chem. Phys.* **1987**, *86*, 2326.

Chart 2

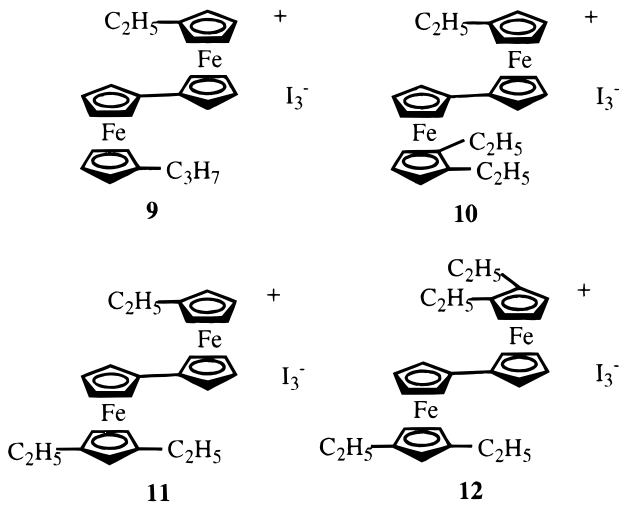

We believe that the most important factor in controlling the intramolecular electron transfer in the series of biferrocenium cations is the symmetry of the cation. We have prepared a series of asymmetric biferrocenium cations (**9**−**12** in Chart 2) to study the influence of zero-point energy difference on electron-transfer rates.[38] The magnitudes of zero-point energy difference between the two vibronic states for asymmetric biferrocenium cations **9**−**12** are nondetectable by electrochemical measurements. However, compounds **9**−**12** show localized Mössbauer characterics at 300 K. Up to the present, no asymmetric biferrocenium cation showing delocalized Mössbauer characterics has been reported.

The observations for the mixed-valence cation **5a** definitively show that the crystallographic properties of the lattice play an important role in controlling the rate of electron transfer. In chemical and biological systems, there are several cases known where slowing solvent molecule motion and lattice dynamics can dramatically affect the rate of electron transfer. In biological systems, protein conformational changes and the motion of amino acid groups have been suggested as providing control and specificity in electron transfer between proteins.[39] Our observation is an interesting result in view of the fact that the crystallographic properties can turn on or off the electron transfer.

Experimental Section

General Information. All manipulation involving air-sensitive materials were carried out by using standard Schlenk techniques under an atmosphere of nitrogen (Scheme 1). Chromatography was performed on neutral alumina (activity II). Solvents were dried as follows: THF and ether were distilled from Na/benzophenone; CH_2Cl_2 was distilled from P_2O_5. The sample of dibromoferrocene was prepared according to the literature procedure.[40]

Synthesis of 1′-Naphthoyl-1-bromoferrocene (7a). Dibromoferrocene (1.72 g, 5 mmol) was placed in a freshly oven-dried three-necked flask (250 mL) and then dried under vacuum at 2 Torr and 30 °C for 4 h. Dried THF (20 mL), followed by butyllithium (3.15 mL; 1.6 M in hexane), was added under nitrogen. The resulting solution was stirred at −25 °C for 30 min, during which 1-lithio-1′-bromoferrocene gradually precipitated. 1-Naphthylnitrile (5 mmol) was then added, and the solution was further stirred at −25 °C for another 25 min. Water (20 mL) was added, and the resulting mixture was extracted with CH_2Cl_2 (50 mL × 2). The combined extracts were dried over sodium sulfate and evaporated at reduced pressure. The residue was chromatographed on a column of neutral alumina (activity II). Elution with hexane gave eluates containing dibromoferrocene and bromoferrocene. Continued elution with ethyl acetate/hexane (1:25) gave eluates that yielded the desired compound (20%). The properties are as follows. ^{1}H NMR ($CDCl_3$, ppm): 8.25 (t, 1H), 7.94 (m, 2H), 7.77 (d, 1H), 7.53 (m, 3H), 4.87 (s, 2H), 4.60 (s, 2H), 4.45 (s, 2H), 4.19 (s, 2H). MS: M^+ at *m*/*z* 418, 420.

Synthesis of 1′-(4-Biphenylcarbonyl)-1-bromoferrocene (7b). The preparation of **7b** (48% yield) was carried out according to the same procedure as the synthesis of **7a**, except using 4-biphenylcarbonitrile as starting material. The physical properties are as follows. ^{1}H NMR ($CDCl_3$, ppm): 8.00 (d, 2H), 7.68 (m, 4H), 7.77 (d, 1H), 7.45 (m, 3H), 5.00 (t, 2H), 4.63 (t, 2H), 4.46 (t, 2H), 4.17 (t, 2H). MS: M^+ at *m*/*z* 444, 446. Mp: 94−96 °C.

Synthesis of 1′-(9-Anthracenecarbonyl)-1-bromoferrocene (7c). The preparation of **7c** (50% yield) was carried out according to the same procedure as the synthesis of **7a**, except using 9-anthraldehyde as starting material. The physical properties are as follows. ^{1}H NMR ($CDCl_3$, ppm): 8.69 (d, 2H), 8.43 (s, 1H), 8.01 (d, 2H), 7.48 (m, 4H), 4.94 (d, 1H), 4.45 (s, 2H), 4.27 (d, 1H), 4.09 (m, 4H), 3.86 (d, 1H), 2.70 (d, 1H). MS: M^+ at *m*/*z* 470, 472. Mp: ∼160 °C (decomp).

Reduction of 7a−**c.** The reduction reaction was carried out by carefully adding, with stirring, small portions of $AlCl_3$ to a mixture of corresponding ferrocene **7** and $LiAlH_4$ in dried ether. After 1 h, the solution became yellow, an excess of H_2O was added to it, and the ether layer was separated. The ether layer was washed with H_2O and dried over $MgSO_4$. After the evaporation of the solvent, the crude product was chromatographed on neutral Al_2O_3, eluting with hexane. The first band was the desired compound **8**.

The physical properties of **8a** (71% yield) are as follows. ^{1}H NMR ($CDCl_3$, ppm): 8.10 (d, 1H), 7.85 (t, 1H), 7.72 (d, 1H), 7.44 (m, 4H), 4.38 (t, 2H), 4.19 (s, 2H), 4.16 (s, 2H), 4.08 (t, 2H). MS: M^+ at *m*/*z* 404, 406. Mp: 113.5−114.5 °C.

The physical properties of **8b** (61% yield) are as follows. ^{1}H NMR ($CDCl_3$, ppm): 7.24−7.57 (m, 9H), 4.37 (s, 2H), 4.18 (d, 4H), 4.10 (s, 2H), 3.80 (s, 2H). MS: M^+ at *m*/*z* 430, 432. Mp: 93.0−95.0 °C.

The physical properties of **8c** (52% yield) are as follows. ^{1}H NMR ($CDCl_3$, ppm): 8.41 (t, 3H), 8.01 (d, 2H), 7.51 (m, 4H), 4.72 (s, 2H), 4.40 (s, 2H), 4.25 (s, 2H), 4.06 (d, 4H). MS: M^+ at *m*/*z* 454, 456. Mp: 135.0−135.5 °C.

Synthesis of 1′,1‴-Disubstituted-biferrocene (6a−**c).** A mixture of corresponding ferrocene **8** (1 g) and activated copper (5 g) was heated under N_2 at 120−130 °C for 24 h. After cooling to room temperature the reaction mixture was repeatedly extracted with CH_2Cl_2 until the CH_2Cl_2 extracts appeared colorless. The extracts were evaporated and chromatographed. The first band eluted with hexane yielded starting material. Continued elution with CH_2Cl_2 afforded the desired compound. The compound could be recrystallized from hexane/benzene.

The physical properties of **6a** (78% yield) are as follows. ^{1}H NMR ($CDCl_3$, ppm): 7.94 (d, 2H), 7.81 (t, 2H), 7.66 (d, 2H), 7.48 (m, 4H), 7.31 (m, 2H), 7.08 (d, 2H), 4.42 (s, 4H), 4.30 (s, 4H), 4.01 (s, 8H), 3.79 (s, 4H). Mass spectrum: M^+ at *m*/*z* 650. Mp: ∼170.0 °C (decomp).

The physical properties of **6b** (75% yield) are as follows. ^{1}H NMR ($CDCl_3$, ppm): 7.14−7.55 (m, 18H), 4.42 (t, 4H), 4.27 (s,

(38) Dong, T.-Y.; Lin, P. J.; Lin, K. J. *Inorg. Chem.* **1996**, *35*, 6037.
(39) (a) Cannon, R. D. *Electron-Transfer Reactions*; Butterworth: London, 1980. (b) Haim, A. *Comments Inorg. Chem.* **1985**, *4*, 113. (c) Jortner, J.; Bixon, M. B. *J. Chem. Phys.* **1988**, *88*, 167. (d) Brown, D. B. *Mixed-Valence Compounds, Theory and Applications in Chemistry, Physics, Geology, and Biology*; Reidel: Boston, MA, 1980. (e) Cannon, R. D.; White, R. P. *Prog. Inorg. Chem.* **1988**, *36*, 195.
(40) Dong, T.-Y.; Lai, L. L. *J. Organomet. Chem.* **1996**, *509*, 131.

4H), 4.00 (s, 8H), 3.48 (s, 4H). MS: M^+ at *m*/*z* 702. Mp: ~155.0 °C (decomp).

The physical properties of **6c** (72% yield) are as follows. ^{1}H NMR ($CDCl_3$, ppm): 8.28 (t, 5.6H), 7.98 (d, 4H), 7.48 (m, 8.5H), 4.62 (d, 4H), 4.44 (s, 8H), 4.17 (q, 4H), 3.95 (s, 4H). MS: M^+ at *m*/*z* 750. Mp: ~215.0 °C (decomp).

Mixed-Valence Compounds 5a−c. A crystalline sample of **5** was prepared by adding a benzene/hexane (1:1) solution containing a stoichiometric amount of iodine to a benzene solution of **6** at 0 °C. The resulting dark green crystals were filtered and washed repeatedly with cold hexane (method 1). A more crystalline sample can be prepared by slowly evaporating the CH_2Cl_2 solution of **5** (method 2) or by slowly diffusing hexane into a saturated CH_2Cl_2 solution of **5** at −10 °C (method 3). Microanalyses of the three different preparations were identical within experimental error.

Anal. Calcd for **5a** ($C_{42}H_{34}Fe_2I_3$): C, 48.92; H, 3.32. Found (method 1): C, 48.88; H, 3.25. Found (method 2): C: 48.84; H, 3.29. Found (method 3): C: 48.93; H, 3.30.

Anal. Calcd for **5b** ($C_{46}H_{38}Fe_2I_3$): C, 51.01; H, 3.54. Found (method 1): C, 51.02; H, 3.53. Found (method 2): C: 50.99; H, 3.55. Found (method 3): C: 51.03; H, 3.53.

Anal. Calcd for **5c** ($C_{50}H_{38}Fe_2I_3$): C, 53.09; H, 3.38. Found (method 1): C, 53.38; H, 3.32. Found (method 2): C: 53.37; H, 3.37. Found (method 3): C, 53.28; H, 3.35.

Physical Methods. ^{57}Fe Mössbauer measurements were made on a constant-velocity instrument, which has been previously described. Computer fitting of the ^{57}Fe Mössbauer data to Lorentzian lines was carried out with a modified version of a previously reported program.[41] Velocity calibrations were made using a 99.99% pure 10 μm iron foil. Typical line widths for all three pairs of iron foil lines fell in the range 0.24−0.27 mm s^{-1}. Isomer shifts are reported relative to iron foil at 300 K but are uncorrected for temperature-dependent, second-order Doppler effects. It should be noted that the isomer shifts illustrated in the figures are plotted as experimentally obtained. Tabulated data are provided.

^{1}H NMR spectra were run on a Varian VXR-300 spectrometer. Mass spectra were obtained with a VG-BLOTECH-QUATTRO 5022 system.

Electrochemical measurements were carried out with a BAS 100W system. Cyclic voltammetry was perform with a stationary glassy carbon working electrode, which was cleaned after each run. These experiments were carried out with a 1×10^{-3} M solution of biferrocene in dry CH_2Cl_2/CH_3CN (1:1) containing 0.1 M $(n\text{-}C_4H_9)_4NPF_6$ as supporting electrolyte. The potentials quoted in this work are relative to a Ag/AgCl electrode at 25 °C.

The single-crystal X-ray determinations of compounds **5a** and **6a** were carried out on an Enraf Nonius CAD4 diffractometer at 298 K. Absorption corrections were made with empirical ψ rotation. Selected bond distances and angles are given in Table 2. Tables of the X-ray crystal data, final positional parameters for all atoms, complete tables of bond distances and angles, and thermal parameters of these compounds are given in the Supporting Information.

Structure Determination of 5a with $P\bar{1}$ Phase. A dark crystal (0.28 × 0.20 × 0.16 mm), which was grown by slow evaporation from a CH_2Cl_2 solution, was used for data collection at 298 K. The $\theta-2\theta$ scan technique was used to record the intensities for all reflections for which $2.16° < \theta < 22.42°$. Of the 2356 unique reflections, there were 2356 reflections with $F_o > 2.0\sigma(F_o^2)$, where $\sigma(F_o^2)$ were estimated from counting statistics. Absorption corrections were applied. These data were used in the final refinement of the structural parameters.

A three-dimensional Patterson synthesis was used to determine the heavy-atom positions, which phased the data sufficiently well to permit location of the remaining non-hydrogen atoms from Fourier synthesis. All non-hydrogen atoms were refined anisotropically. Hydrogen atoms were calculated at ideal distances. The greatest residual electron density upon completion of refinement was in the vicinity of the iodide atoms. Final residuals were R1 = 0.0354 and wR(f^2) = 0.0875.

Structure Determination of 5a with $P2_1/n$ Phase. A dark black crystal (0.34 × 0.24 × 0.24 mm) was obtained when a layer of hexane was allowed to slowly diffuse into a CH_2Cl_2 solution of **5a**. Data were collected with θ in the range 1.43−22.43°. The data were also corrected for absorption with an empirical ψ rotation. Of the 4764 unique reflections, there were 3289 with $F_o^2 > 2.0\sigma(F_o^2)$. These data were used in the final refinement of the structural parameters. Structure refinement was carried out in the same manner as described above. Final residuals were R1 = 0.0348 and wR(f^2) = 0.0980.

Structure Determination of 6a. An orange crystal (0.32 × 0.28 × 0.26 mm) was obtained by slow evaporation from a CH_2Cl_2 solution. Data were collected with $3.74° < 2\theta < 44.84°$. Of the 1955 unique reflections, there were 1955 with $F_o > 2.0\sigma(F_o^2)$. These data were used in the final refinement of structural parameters. The structure was solved and refined as described for **5a**. Final residuals were R1 = 0.0260 and wR(f^2) = 0.0703.

Acknowledgments are made to the National Science Council (NSC89-2113-M-110-003), Taiwan, ROC, and Department of Chemistry at Sun Yat-Sen University.

Supporting Information Available: Complete tables of crystal data, positional parameters, bond lengths and angles, and thermal parameters for **5a** and **6a**. This material is available free of charge via the Internet at http://pubs.acs.org.

OM9908884

(41) Lee, J. F.; Lee, M. D.; Tseng, P. K. *Chemistry* **1987**, *45*, 50.